Phase evolution of solid-state $BaTiO_3$ powder prepared with the ultrafine $BaCO_3$ and TiO_2

Ting-Tai Lee
Department of Resources Engineering, National Cheng Kung University, Tainan 70101, Taiwan; and MLCC R & D Division, Yageo Corporation, Kaohsiung 81170, Taiwan

Chi-Yuen Huang[a] and Che-Yuan Chang
Department of Resources Engineering, National Cheng Kung University, Tainan 70101, Taiwan

I-Kuan Cheng, Ching-Li Hu, Chun-Te Lee, and Masayuki Fujimoto
MLCC R&D Division, Yageo Corporation, Kaohsiung 81170, Taiwan

(Received 3 May 2012; accepted 28 June 2012)

The phase evolution, nucleation, and sintered ceramics of barium titanate ($BaTiO_3$, BT) powder prepared by solid-state synthesis with an ultrafine starting material (27 m^2/g of $BaCO_3$ and 190 m^2/g of TiO_2) were investigated in this study. Surface diffusion between $BaCO_3$ and TiO_2 was observed at a relatively low temperature of 400 °C by transmission electron microscopy. Rapid nucleation of the BT and cubic BT phases was observed at 500 °C by x-ray diffraction. The derivative thermogravimetry curve clearly shows a single step of BT formation at 600 °C. In short, pure BT particles with an average particle size of 250 nm and high tetragonality were prepared by solid-state synthesis, which produced X7R ceramics with high dielectric permittivity, high insulation resistance, and a clear core–shell structure.

I. INTRODUCTION

A small, uniform, and well-dispersed barium titanate ($BaTiO_3$, BT) powder is needed for use as the dielectric material in multilayer ceramic capacitors (MLCCs) with ultrathin active layers.[1–5] Two main challenges in the current development of MLCCs are the trends for both smaller size (miniaturization) and greater capacitance values. For example, the number of dielectric layers in one capacitor now often exceeds 1000, and a thickness of less than 1 μm for each active layer is required.

Solid-state BT has the advantages of good crystallinity, low cost, and high precision of stoichiometric control. The phase evolution of solid-state BT has been studied by many researchers.[6–17] Beauger et al.[10,11] built a model that explains how barium ions diffuse though the TiO_2 surface and control BT growth. Rössel et al.[15] used Raman spectral imaging to confirm the mechanism by which the BT layer continues to form and consumes the TiO_2 surface. Kobayashi and Lee[16,17] reported the presence of a thin layer of BT on a rutile TiO_2 surface and confirmed the existence of Ba–Ti–O precursor and nucleation through in situ transmission electron microscopy (TEM) observations. With regard to the mixing mechanism used to prepare the solid-state BT, Hennings et al.[1,18,19] reported that BT with a low calcination temperature and a pure crystal phase (without the secondary phase, Ba_2TiO_4) can achieve the viscosity stability of an aqueous slurry in the MLCC process. Ando et al.[20,21] used high-energy bead milling to prepare finer BT and proposed a two-step (nucleation → BT particle growth) schematic model of BT formation. Three important factors for solid-state BT synthesis have been proposed: an increase in contact point density between $BaCO_3$ and TiO_2, the enhanced formation rate of nucleation, and a decrease in the diffusion path due to the size reduction of the starting material after mixing. Buscaglia et al.[22,23] prepared nanocrystalline BT with a single phase and high tetragonality using starting materials with different particle sizes and the traditional ball milling method. They also introduced a kinetic model of nucleation and growth to explain the three steps (nucleation → BT particle growth → final reaction for TiO_2 agglomerate residual) of solid-state BT formation derived from the weight loss curves. In our previous work,[17] we observed the phase evolution of solid-state BT with the standard-sized $BaCO_3$ (2 m^2/g) and TiO_2 (7 m^2/g) and prepared 500-nm BT particles. We also observed the formation of an intermediate phase of Ba_2TiO_4, nucleation of BT, and the physical properties of their sintered ceramics. According to the reports of Hennings et al.[19] and Buscaglia et al.,[22] a low calcination temperature of about 800 °C can suppress the formation of Ba_2TiO_4.

The aim of this study was the preparation of solid-state BT (with an average particle size of less than 250 nm) with high tetragonality with the use of ultrafine starting materials, $BaCO_3$ (27 m^2/g) and TiO_2 (190 m^2/g). We

[a]Address all correspondence to this author.
e-mail: cyhuang@mail.ncku.edu.tw
DOI: 10.1557/jmr.2012.255

 © Materials Research Society 2012

https://doi.org/10.1557/jmr.2012.255 Published online by Cambridge University Press

anticipated that the relatively low synthesized temperature could prevent the formation of a secondary phase. We are also interested in the phase evolution and morphology of BT, which are examined using in situ TEM analysis. Furthermore, the dielectric properties of the ceramics should satisfy the X7R-MLCCs' requirement (Electric Industries Association standard: the tolerance of capacitance from −55 to +125 °C is ±15%), and these are also examined in this work.

II. EXPERIMENTAL

The starting materials, i.e., reagent grade $BaCO_3$ (needle type, S_{BET} = 27 m^2/g) and TiO_2 (S_{BET} = 190 m^2/g for 100% rutile phase), were mixed in water with a commercial high-energy bead mill with 0.1 mm media. Low molecular weight ammonium polyacrylate (Antiprex A40; Ciba, Switzerland) was used for dispersion. The Ba/Ti molar ratio was set at 1.001 through the stoichiometric method. The mixed slurry was dried at 130 °C for 24 h and pulverized. The raw powder mixture was investigated for its kinetic reaction by simultaneous thermogravimetry and differential scanning calorimetry (DSC, STA449C; Netzsch, Selb, Germany) after sieving with a 50 mesh. To examine BT formation, the raw mixture powder was loaded in a ceramic crucible and calcined at different peak temperatures (400–1000 °C) for 2 h with an air atmosphere in a batch furnace (heating rate 8 °C/min). The specific surface areas (SSAs) (S_{BET}) of the raw mixture powder and BT were detected using Brunauer, Emmett, and Teller's (BET) method (Model ASAP 2010; Micromeritics, Norcross, GA). The $6/\rho S_{BET}$ equation was used to obtain the equivalent BET diameter (d_{BET}). The morphology, chemical composition, particle size, and microstructure of the BT raw mixture and sintered ceramics were then determined by cold field-emission (scanning) TEM with high-angle annular dark field imaging (HAADF) and an energy-dispersive x-ray spectroscope (EDS) (HF3300, Hitachi America, Pleasanton, CA) and field-emission gun scanning electron microscopy (FE-SEM, Nova Nano-SEM 230; FEI, Hillsboro, OR). A dispersed powder sample on a carbon-coated microgrid was also used for TEM sample preparation. A focused ion beam system was one of the methods used in this work for the TEM sample preparation of thin section of sintered ceramics. The phase identification of the raw material and calcined powder was undertaken by x-ray diffraction (XRD; PW3040, X'Pert MPD, PANalytical, Almelo, Netherlands) analysis. Diffractive data were refined using TOPAS 3.0 (Bruker AXS, Karlsruhe, Germany) to obtain the crystal structure and lattice parameter calculation. The Ba/Ti molar ratio of the BT sample was identified using a sequential x-ray fluorescence spectrometer (XRF, S8 TIGER/A15-X10; Bruker AXS). Calcined BT powder was mixed with commercial dopant oxides of X7R formulation, including Y, Mn, and Si. Drying, granulation, and isostatic pressing were used for the preparation of ceramic pellets. Green pellets were sintered at 1250 °C for 2 h in wet H_2 (P_{O2} = 10^{-13}–10^{-14} atm) by a base metal electrode MLCC process. The sintering conditions were optimized to reveal the grain size and core–shell structure. The density of the fired ceramics was obtained by Archimedes' method. A Cu electrode covered both sides of the pellet at 800 °C. The temperature coefficient of capacitance (TCC) was measured at 1 kHz and 1 V_{rms} from −55 to 150 °C using an automated system for heating (VTM7044; Vötsch, Berlin, Germany) and capacitance detection (LCR meter E4980A, Agilent, Santa Clara, CA). The capacitance and loss factor ($\varepsilon_r \tan \delta$) were measured using a LCR meter 4268A. The insulation resistance (IR) was measured with a high-resistance meter (Agilent 4339B).

III. RESULTS AND DISCUSSION

A. Derivative thermogravimetry/DSC analysis

The DSC and derivative thermogravimetry (DTG) (first derivative of weight loss) curves of the mixture with a constant heating rate (5 °C/min) are reported in Fig. 1. The DSC peak position can fit the position of the DTG peak. Only one endothermic peak is shown at 640 °C. In previous report,[16–23] the presence of residual and agglomerates of TiO_2 in the mixture should dominate the existence of surplus DTG peaks and the agglomerates will need a higher temperature for calcination to obtain a pure BT. In our starting material, the equivalent BET diameter of TiO_2 (190 m^2/g) is 8 nm, and for $BaCO_3$ (27 m^2/g), it is 52 nm. Compared with the DTG reactions proposed in the previous reports, no surplus reactions occurring over 600 °C were observed in our mixture system. A single step reaction of BT formation is obtained in this study through the decrease in particle size and the mixing process using a high-energy bead mill.

Kubo and Shinriki[7,8] and Niepce and Thomas[14] reported a three-step reaction to synthesize BT: a thin layer of BT was first observed on the surface of TiO_2, then the

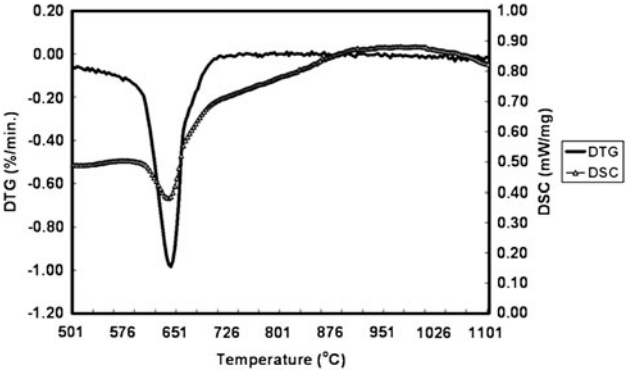


FIG. 1. DSC and DTG curves for $BaCO_3$ and TiO_2 mixtures. Heating rate: 5 °C/min.

https://doi.org/10.1557/jmr.2012.255 Published online by Cambridge University Press

Ba_2TiO_4 phase was formed between BT and $BaCO_3$ during the solid-state reaction of $BaCO_3$ and TiO_2, and then BT was fully synthesized. In our previous work, the presence of a thin layer of BT on a rutile TiO_2 surface was also reported based on TEM observations.[17] According to these reports, 600 °C may be a critical point for the first step of BT formation in solid-state synthesis, regardless of the effects of the particle size of the starting material or mixing mechanism used, as the solid-state reaction and nucleation of BT may occur at this temperature. In this study, the results of the XRD and TEM analyses will help to clarify the process of BT formation at a lower calcination temperature of 400–600 °C with an ultrafine starting material.

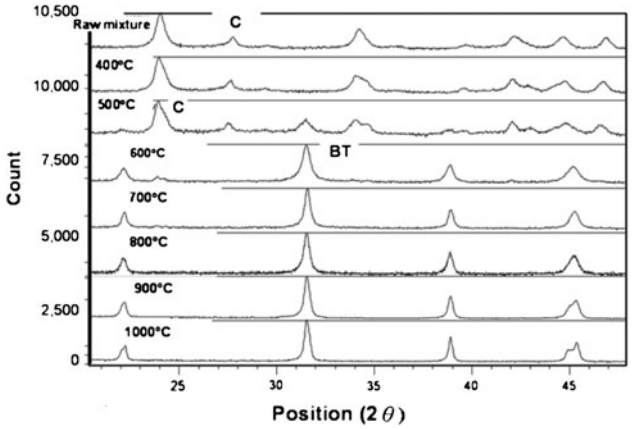


FIG. 2. XRD patterns of BT raw mixture at different calcination temperatures in air atmosphere (400–1000 °C) for 2 h. C, $BaCO_3$; BT, $BaTiO_3$.

B. Characterization of raw mixture and calcined powders

1.001 of the Ba/Ti molar ratio was detected at different calcination temperatures by XRF. The raw mixture was calcined from 400 to 1000 °C for 2 h in air, and the XRD patterns for phase identification are shown in Fig. 2. Two phases, i.e., $BaCO_3$ and BT, were detected. The intensity of ultrafine TiO_2 (rutile phase) became weaker, and the broadened (110) peak of TiO_2 was not separated easily from the (021) peak of $BaCO_3$. In the second phase, Ba_2TiO_4 was clearly observed during the solid-state reaction by the traditional mixing process, but it was not detected in our raw mixture system by XRD. The starting materials were only detected at temperatures of 400 °C, and no intermediate phases were observed. The BT crystal phase started to form at 500 °C, and significant decreases in the intensities of $BaCO_3$ were observed at 600 °C. At the same time, the intensity of the BT phase dramatically increased. A pure cubic phase of BT was obtained at 800 °C, and a pure tetragonal phase (c/a ratio $>$ 1.006) of

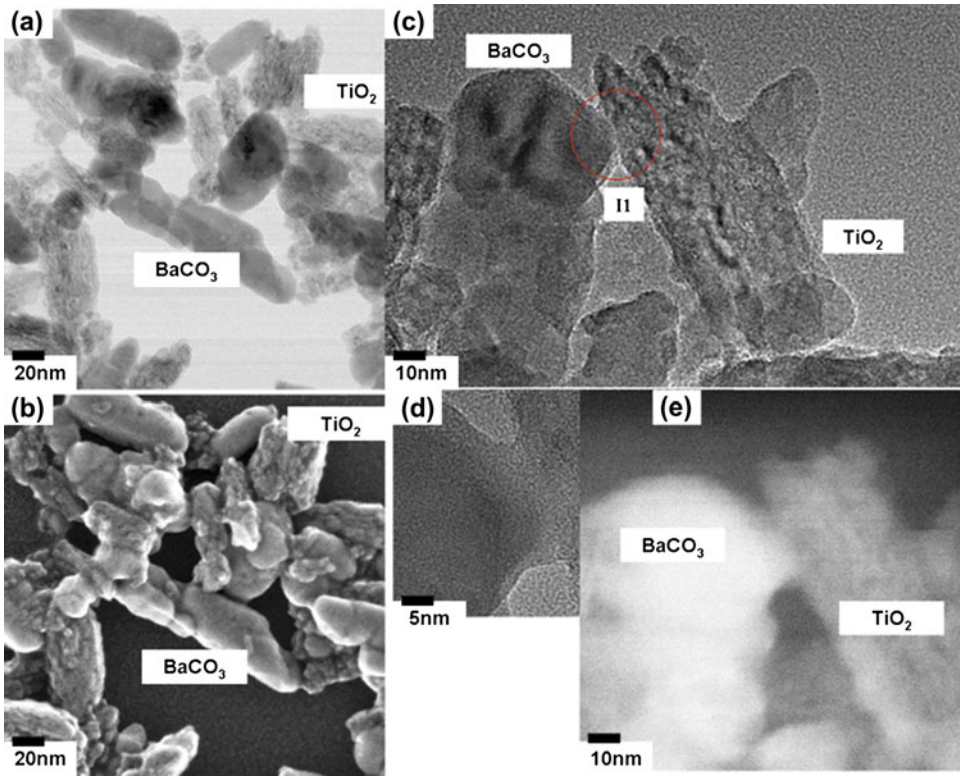


FIG. 3. TEM images of powder sample: (a) transmitted electron, (b) secondary electron images of raw mixture, (c) transmitted electron, (d) high resolution, and (e) HAADF images of the sample calcined at 400 °C in I1 area.

https://doi.org/10.1557/jmr.2012.255 Published online by Cambridge University Press

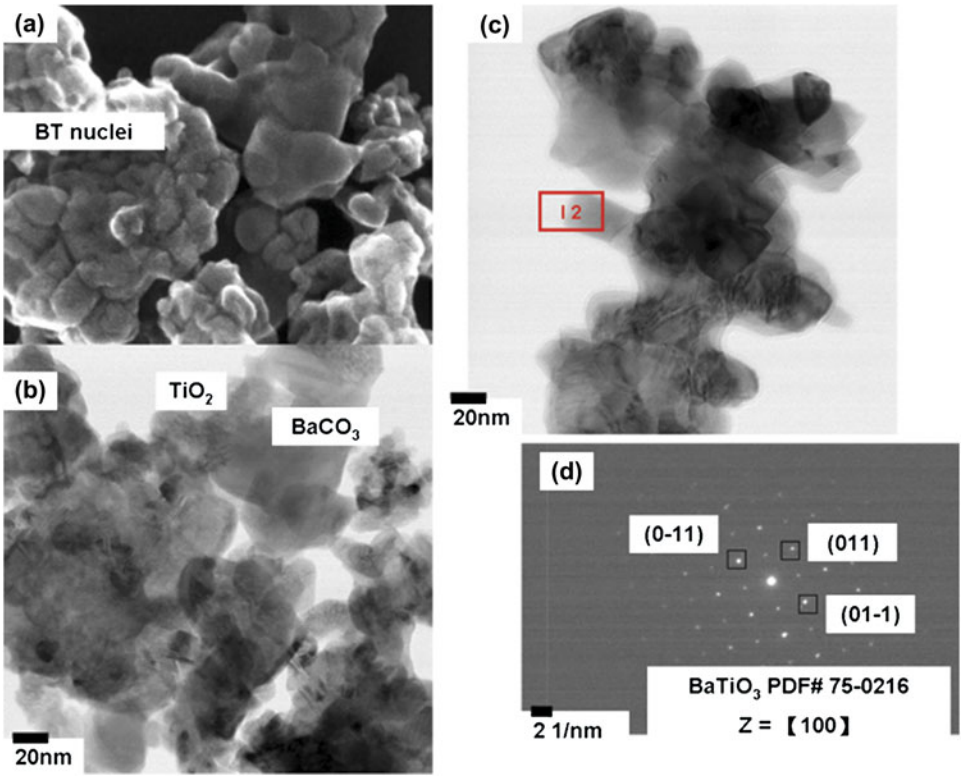


FIG. 4. TEM images of powder sample: (a) secondary electron, (b) transmitted electron images of sample calcined at 500 °C, (c) transmitted electron image, and (d) selected area diffraction pattern of the sample calcined at 600 °C.

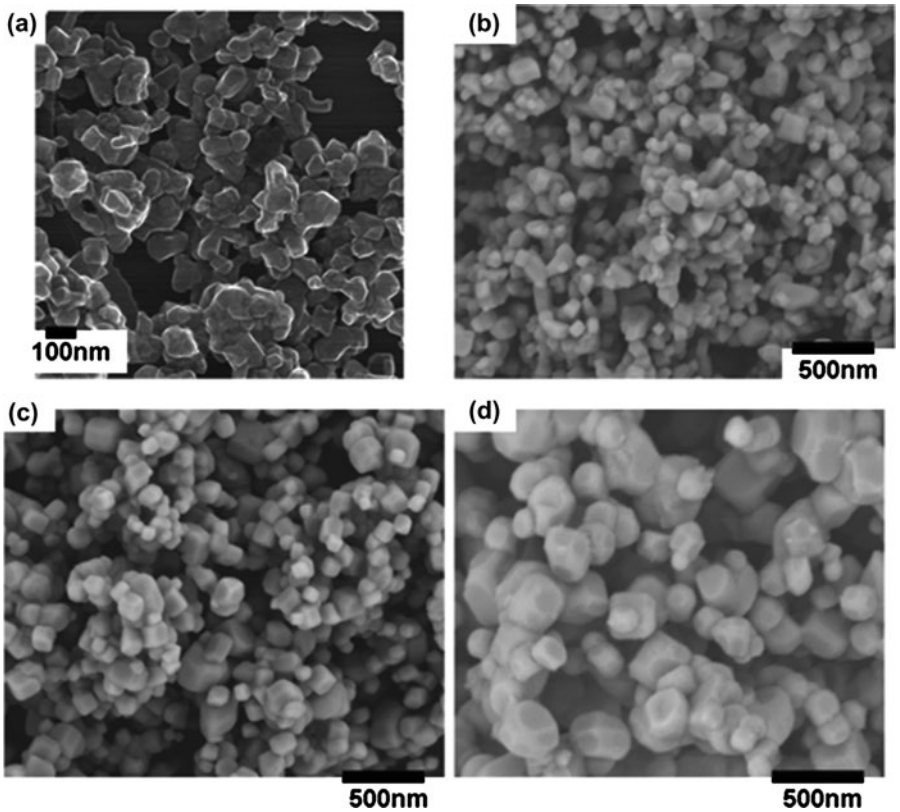


FIG. 5. Morphologies (obtained by TEM and FE-SEM) of powder sample calcined at (a) 700 °C, (b) 800 °C, (c) 900 °C, and (d) 1000 °C for 2 h.

https://doi.org/10.1557/jmr.2012.255 Published online by Cambridge University Press

BT was obtained at 900 °C with separate (002) and (200) peaks. Finally, tetragonal BT ($c/a > 1.007$) was obtained at 1000 °C.

The TEM images clearly show the morphologies of the raw mixture with different calcination temperatures (Fig. 3). Figures 3(a) and 3(b) show the different morphologies of the $BaCO_3$ and TiO_2 particles in the raw mixture. The TEM images show that the $BaCO_3$ was composed of two or three columnar particles with smooth surfaces. After the bead milling, the $BaCO_3$ particles were crushed and cut into shorter and broken particles with a size of about 30 nm. The TiO_2 was found as agglomerate particles with a spindle shape composed of many 2–3 nm spherical particles. With calcination at 400 °C, necking between the $BaCO_3$ and TiO_2 particles was observed under high resolution and HAADF imaging [Figs. 3(c) and 3(d)]. In Fig. 3(e), the bright and dark areas indicate the surface diffusion between $BaCO_3$ and TiO_2 particles (I1 area). Because barium (Ba) has an atomic number of 56, which is higher than that of titanium (Ti), which is 22, a different mass-contrast image was used for analysis of the qualitative element distribution. The results show a clear diffusion layer at 400 °C due to the surface diffusion between $BaCO_3$ and TiO_2.

When the calcination temperature increased to 500 °C, a clear (110) peak was observed by XRD (Fig. 2), indicating the cubic BT phase. Significant BT nucleation was also observed in Fig. 4(a). In the TEM image [Fig. (4b)], we can separate the $BaCO_3$ and TiO_2 based on their distinctive morphologies, and many nanoparticles and defects were observed in these BT nuclei. A broadening (110) peak of XRD can also be seen, indicating that fine crystallites of BT formed at 500 °C compared to the sample produced at a higher calcination temperature, based on Scherrer's equation. BT formation and growth occurs at this stage, even though we can not obtain a clear selected diffraction pattern from the TEM analysis to confirm whether these BT nuclei were cubic BT. However, the data from DTG and XRD analyses suggest that the rapid formation of BT occurred due to the use of ultrafine TiO_2.

Twenty-nanometer cubic BT without lattice defects was obtained at 600 °C [Fig. 4(c)], while a weak $BaCO_3$ peak was still detected at this calcination temperature (Fig. 2). The selected area diffraction pattern shown in Fig. 4(d) demonstrates that the unitary particles of cubic BT formed with a spot pattern belonging to the space group *Pm3m* (No. 75-0216). At 700 °C, BT particles were grown with a size ranging from 50 to 80 nm with a narrow particle size distribution [Fig. 5(a)], and the nuclei crystallites disappeared at this temperature. The XRD results show that a residual $BaCO_3$ peak was still detected at this calcination (Fig. 2). FE-SEM was used to observe the BT morphology from 800 to 1000 °C. When the calcination temperature rose to 800 °C, a pure cubic BT phase with an average particle size of 120 nm was obtained [Fig. 5(b)]. A pure tetragonal phase (c/a ratio > 1.006) of BT was obtained at 900 °C, with an average particle size of 150 nm [Fig. 5(c)]. Finally, a pure tetragonal BT ($c/a > 1.007$) was obtained at 1000 °C, with an average particle size of 250 nm [Fig. 5(d)]. The SSA and equivalent BET diameters of the raw mixture and calcined BT are shown in Table I.

TABLE I. SSAs of calcined BT powders.

Calcination temperature (°C)	Specific surface area, BET (m^2/g)	Equivalent BET diameter (nm)
Raw mixture	46.18	...
400	33.26	...
500	21.45	...
600	15.43	...
700	10.95	...
800	8.12	122
900	6.55	152
1000	3.99	250

C. Electric properties of ceramics

Relative densities of more than 95% are shown in Table II for the sintered ceramics prepared from the BT samples obtained at calcination temperatures of 900 and 1000 °C because the pure tetragonal BT phase was obtained at these two conditions. The theoretical density was assumed to be 6.02 g/cm^3. According to the temperatures of the relative dielectric permittivity curves and TCC curves [Figs. 6(a) and 6(b)], the 900 and 1000 °C calcination samples have the typical core–shell properties of the X7R ceramic.[24–27] The Curie point was at 125 °C for both samples, while the dielectric loss curves show clear turning points at −53 and 125 °C, and these should belong to the phase transition of BT. The two samples showed a similar trend that the dielectric loss decreased with the increase in temperature. With 900 °C sample, there are two more turn points at −9 and 95 °C in the dielectric loss curve, and these may show the dielectric properties of the solid solution during the diffuse phase transition between

TABLE II. Characteristics of ceramic pellets from different calcined BT powders sintered at 1250 °C for 2 h in wet H_2.

Calcination temperature (°C)	Average grain size (nm)	Relative density (%)	Relative permittivity	Loss tan δ ($\times 10^{-4}$)		IR (MΩ)
				Min	Max	
900	189	98	2072	44	47	1.0307×10^6
1000	313	98	2967	73	76	1.0972×10^6

https://doi.org/10.1557/jmr.2012.255 Published online by Cambridge University Press

the finer BT and the dopants.[28] However, both the two samples could satisfy the X7R specifications [Fig. 6(b)]. A relative permittivity of 2100 and a loss factor of 0.4% at room temperature were obtained for the 900 °C sample. The 1000 °C calcined sample had a higher dielectric permittivity ($\varepsilon_r \sim 3000$), but a higher loss factor (0.7%) was detected at room temperature. The dielectric permittivity and loss factor increased along with the BT calcination temperature. Tsurumi et al.[4] reported that greater dielectric permittivity was obtained with a higher density and tetragonality of fine BT particles. The defects that cause a low dielectric permittivity, such as grain boundary, internal surfaces and nanopores, dislocations, and OH lattice defects, should not be found inside the BT particles. At the solid state synthesized BT samples in this study, all these defects may be eliminated with calcination at temperatures from 600 °C up. Furthermore, both the samples had an IR that was higher than 10^6 MΩ.

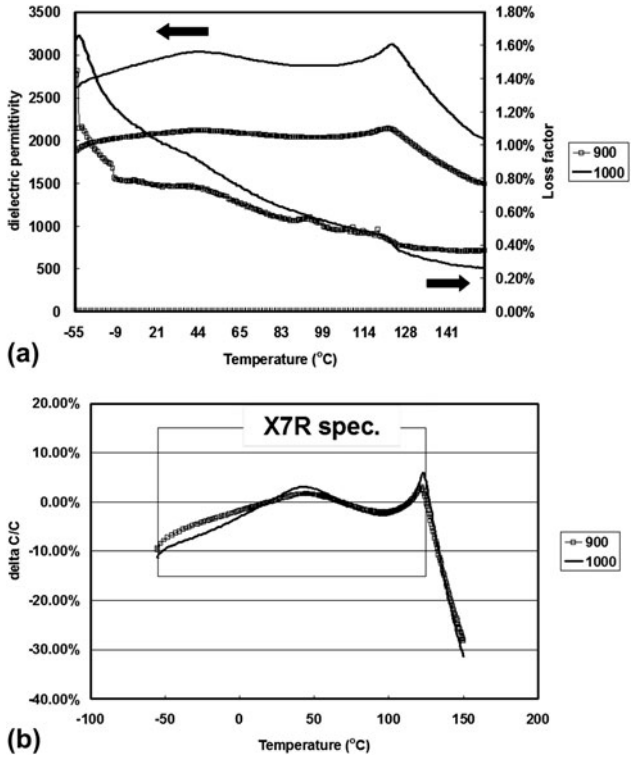


FIG. 6. (a) Temperature dependences of the relative dielectric permittivity and loss factor and (b) TCC curves. The ceramic pellets were from the powder samples calcined at 900 and 1000 °C.

Figures 7 and 8 are SEM and TEM micrographs, respectively, which show the grain size distribution and core–shell structure in a BT grain sintered in a reducing atmosphere (1250 °C for 2 h in wet H_2). The grain size is clearly revealed after effective thermal etching (1100 °C for 30 min), and the average grain size is 189 nm for the 900 °C sample and 313 nm for the 1000 °C sample. A fully dense and homogeneous grain size distribution was obtained in both samples. The grain growth occurred during the sintering. Compared to the particle size of BT powder (Table I), the increase in grain size is 24% and 25% for 900 and 1000 °C samples, respectively. The core–shell structure in a BT grain, as observed by TEM, is shown in Fig. 8. Base on previous reports,[4,5,24–29] the core region reveals a pure tetragonal BT with ferroelectric properties, and the paraelectric pseudocubic shell is consists of solid solution with BT and dopants. In typical TCC curves of X7R material, the high dielectric permittivity of the Curie point is a property of the core, whereas the shell has low dielectric permittivity at room temperature. The diffuse phase transition leads to the X7R feature of a stable dielectric constant with regard to temperature. In Fig. 8(b), a core region with a domain structure that is covered by a shell without a domain structure can be clearly seen in the 1000 °C sample. Compared to the 900 °C sample [Fig. 8(a)], it is slightly easier to find a complete core–shell structure in the 1000 °C sample. One of the dopant elements, Yttrium (Y), is detected by scanning-transmission electron microscopy with energy dispersive x-ray spectroscopy (STEM-EDS), and its distribution is shown in Figs. 8(c) and 8(d). Y is located in the shell

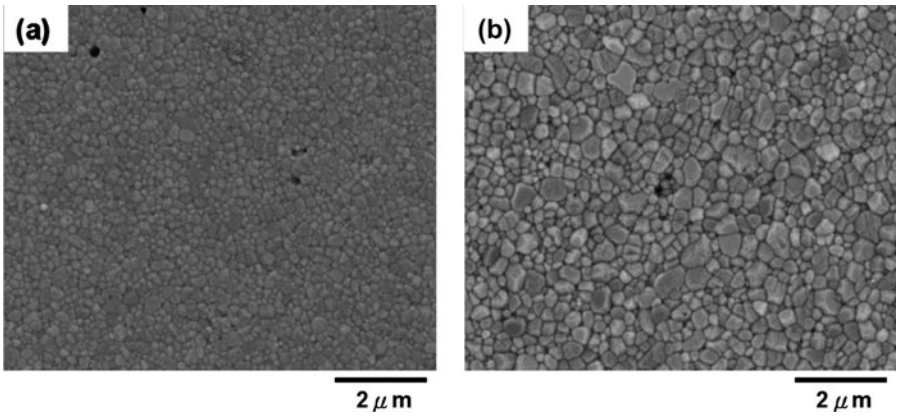


FIG. 7. FE-SEM micrographs of the ceramic pellets sintered at 1250 °C for 2 h in wet H_2 for the powder samples calcined at (a) 900 °C and (b) 1000 °C.

https://doi.org/10.1557/jmr.2012.255 Published online by Cambridge University Press

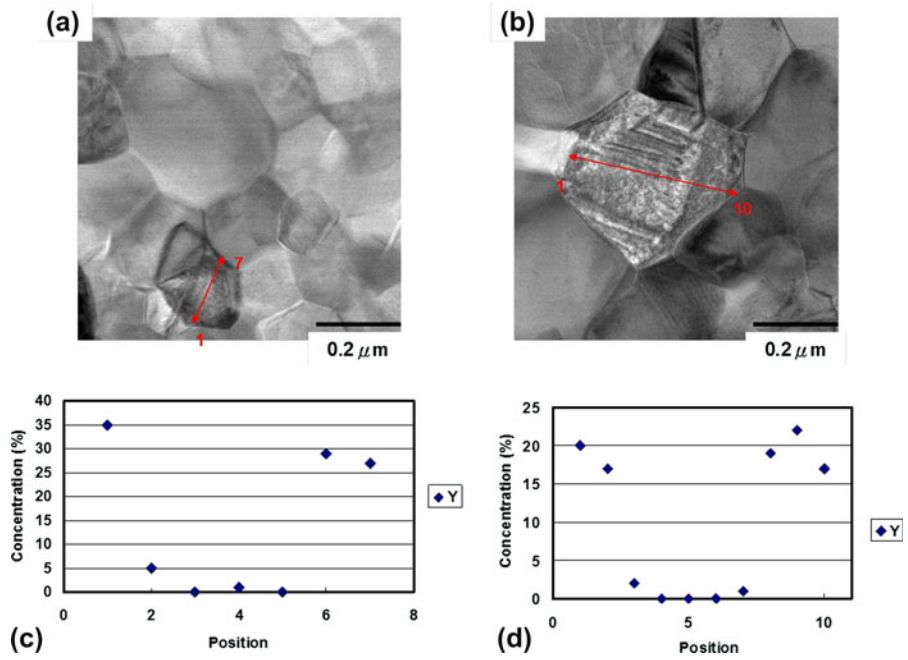


FIG. 8. TEM micrographs of the ceramic pellets sintered at 1250 °C for 2 h in wet H_2 for the powder samples calcined at (a) 900 °C and (b) 1000 °C; their STEM-EDS line profiles for the core–shell structures: (c) 900 °C and (d) 1000 °C, showing the distribution of Y.

region and grain boundary, whereas the absence of Y is observed in the core region. In previous reports,[5,25,27] Mg and Y were the basic elements forming the shell region in a BT grain through the solid-state diffusion or a dissolution/precipitation mechanism.[24,26] In our observation, the finer grain distribution of the 900 °C sample has a lower dielectric constant with fewer domain walls in the core–shell structure, and the nonhomogeneous distribution of the shell and core regions may be one of reasons for this. A good dispersion between dopants and finer BT particles, and a suitable sintering process, should thus be helpful to improve the dielectric properties in finer BT system.

In conclusion, using the approach described in this work, BT particles with an average particle size of 250 nm and high tetragonality were prepared by solid-state synthesis, which produced X7R ceramics with high dielectric permittivity, high IR, and a clear core–shell structure.

IV. CONCLUSIONS

The present study investigated the phase evolution and nuclei growth of solid-state BT powder and the dielectric properties of the related ceramics with an ultrafine starting material. The results of the DTG curve for a mixture of $BaCO_3$ and TiO_2 clearly showed that there was only one reaction step at 600 °C. Surface diffusion between $BaCO_3$ and TiO_2 was clearly observed at a relatively low temperature of 400 °C. The rapid formation of BT nuclei and the cubic BT phase was observed at 500 °C by XRD and TEM. At 800 °C, a pure cubic BT phase with an average particle size of 120 nm was obtained. A pure tetragonal phase (c/a ratio > 1.006) of BT was obtained at 900 °C, with an average particle size of 150 nm. Finally, a pure tetragonal BT phase ($c/a > 1.007$) was obtained at 1000 °C, with an average particle size of 250 nm. The temperature–dielectric permittivity and TCC curves reveal the X7R (core/shell) dielectric properties of the 900 and 1000 °C sample ceramics. A relative permittivity of 2100 and a loss factor of 0.4% at room temperature were found for the 900 °C sample. The 1000 °C calcined sample had higher dielectric permittivity ($\varepsilon_r \sim 3000$) and a greater loss factor (0.7%) at room temperature, and a high IR of 10^6 MΩ was obtained. A core–shell structure rich in Y in the shell region was also observed in this study. In short, single phase 120-nm cubic BT and 250-nm tetragonal BT particles, which produced ceramics with high dielectric permittivity and IR, were obtained in this study.

ACKNOWLEDGMENTS

T-T.L. would like to thank Yageo Corporation for supporting the Ph.D. program. This work was supported by the National Science Council of Taiwan under Contract No. NSC 100-2221-E-006-134-MY3.

REFERENCES

1. C. Pithan, D. Hennings, and R. Waser: Progress in the synthesis of nanocrystalline $BaTiO_3$ powders for MLCC. *Int. J. Appl. Ceram. Technol.* **2**, 1 (2005).
2. H. Kishi, Y. Mizuno, and H. Chazono: Base-metal electrode-multilayer ceramic capacitors: Past, present and future perspectives. *Jpn. J. Appl. Phys.* **42**, 1 (2003).

https://doi.org/10.1557/jmr.2012.255 Published online by Cambridge University Press

3. C.A. Randall: Scientific and engineering issues of the state-of-art and future multilayer ceramic capacitors. *J. Ceram. Soc. Jpn.* **109**, S2 (2001).
4. T. Tsurumi, T. Sekine, H. Kakemoto, T. Hoshina, S-M. Nam, H. Yasuno, and S. Wada: Evaluation and statistical analysis of dielectric permittivity of $BaTiO_3$ powders. *J. Am. Ceram. Soc.* **89**, 1337 (2006).
5. Y. Mizuno, T. Hagiwara, and H. Kishi: Microstructural design of dielectrics for Ni-MLCC with ultra-thin active layers. *J. Ceram. Soc. Jpn.* **115**, 360 (2007).
6. W. Trzebiatowski, J. Wojciechowska, and J. Damm: Mechanism of synthesis of barium titanate. *Roczniki Chem.* **26**, 12 (1952).
7. T. Kubo and K. Shinriki: Chemical reaction in the solid state: III, Reaction between $BaCO_3$ and TiO_2 in solid state. *J. Chem. Soc. Jpn.* **55**, 49 (1952).
8. T. Kubo and K. Shinriki: Chemical reaction in the solid state: IV, Interface of moisture and carbon dioxide on formation of various barium titanates. *J. Chem. Soc. Jpn.* **55**, 137 (1952).
9. L.K. Templeton and J.A. Pask: Formation of $BaTiO_3$ from $BaCO_3$ and TiO_2 in air and in CO_2. *J. Am. Ceram. Soc.* **42**, 212 (1959).
10. A. Beauger, J.C. Mutin, and J.C. Niepce: Synthesis reaction of metatitanate $BaTiO_3$. Part 1. Effect of the gaseous atmosphere upon the thermal evolution of the system $BaCO_3$ – TiO_2. *J. Mater. Sci.* **18**, 3041 (1983).
11. A. Beauger, J.C. Mutin, and J.C. Niepce: Synthesis reaction of metatitanate $BaTiO_3$. Part 2. Study of solid-solid reaction interfaces. *J. Mater. Sci.* **18**, 3543 (1983).
12. A. Amin, M.A. Spears, and B.M. Kulwicki: Reaction of anatase and rutile with barium carbonate. *J. Am. Ceram. Soc.* **66**, 733 (1983).
13. W. Hertl: Kinetics of barium titanate synthesis. *J. Am. Ceram. Soc.* **71**, 879 (1988).
14. J.C. Niepce and G. Thomas: About the mechanism of the solid way synthesis of barium metatitanate. Industrial consequences. *Solid State Ionics* **43**, 69 (1990).
15. M. Rössel, H.R. Höche, H.S. Leipner, D. Völtzke, H.P. Abicht, O. Hollricher, J. Müller, and S. Gablenz: Raman microscopic investigations of $BaTiO_3$ precursors with core-shell structure. *Anal. Bioanal.Chem.* **380**, 157 (2004).
16. K. Kobayashi, T. Suzuki, and Y. Mizuno: Microstructure analysis of solid-state reaction in synthesis of $BaTiO_3$ powder using transmission electron microscope. *Appl. Phys. Express* **1**, 041602 (2008).
17. T.T. Lee, C.Y. Huang, C.Y. Chang, S.P. Lin, C.Y. Su, C.T. Lee, and M. Fujimoto: Phase evolution and nucleus growth observation of solid-state $BaTiO_3$ powder prepared by high-energy bead milling for raw material mixing. *Jpn. J. Appl. Phys.* **50**, 091502 (2011).
18. W.S. Lee, D.F.K. Hennings, and T.Y. Tseng: Effect of calcination temperature and A/B-ratio on dielectric properties of (Ba, Ca) (Ti, Zr, Mn)O_3 multilayer capacitors with Ni electrodes. *J. Am. Ceram. Soc.* **83**, 1402 (2000).
19. D. Hennings, B. Seriyati Schreinemacher, and H. Schreinemacher: Solid–state preparation of $BaTiO_3$-based dielectrics using ultrafine raw materials. *J. Am. Ceram. Soc.* **84**, 2777 (2001).
20. C. Ando, R. Yanagawa, H. Chazono, H. Kishi, and M. Senna: Nuclei-growth optimization for fine-grained $BaTiO_3$ by precision-controlled mechanical pretreatment of starting powder mixture. *J. Mater. Res.* **19**, 3592 (2004).
21. R. Yanagawa, M. Senna, C. Ando, H. Chazono, and H. Kishi: Preparation of 200 nm $BaTiO_3$ particles with their tetragonality 1.010 via a solid-state reaction preceded by agglomeration-free mechanical activation. *J. Am. Ceram. Soc.* **90**, 809 (2007).
22. M.T. Buscaglia, M. Bassoli, V. Buscaglia, and R. Alessio: Solid-state synthesis of ultrafine $BaTiO_3$ powders from nanocrystalline $BaCO_3$ and TiO_2. *J. Am. Ceram. Soc.* **88**, 2374 (2005).
23. M.T. Buscaglia, M. Bassoli, V. Buscaglia, and R. Vormberg: Solid-state synthesis of nanocrystalline $BaTiO_3$: Reaction kinetics and powder properties. *J. Am. Ceram. Soc.* **91**, 2862 (2008).
24. D. Hennings and G. Rosenstein: Temperature-stable dielectrics based on chemically inhomogeneous $BaTiO_3$. *J. Am. Ceram. Soc.* **67**, 249 (1984).
25. H. Kishi, Y. Okino, M. Honda, Y. Iguchi, M. Imada, Y. Takahashi, H. Ohsato, and T. Kuda: The effect of MgO and rare-earth oxide on formation behavior of core-shell structure in $BaTiO_3$. *Jpn. J. Appl. Phys.* **36**, 5954 (1997).
26. C.A. Randall, S.F. Wang, D. Laubscher, J.P. Dougherty, and W. Huebner: Structure property relationships in core-shell $BaTiO_3$–LiF ceramics. *J. Mater. Res.* **8**, 871 (1993).
27. T. Wang, X.H. Wang, H. Wen, and L.T. Li: Effect of milling process on the core-shell structures and dielectric properties of fine-grained $BaTiO_3$-based X7R ceramic materials. *Int. J. Miner. Metall. Mater.* **16**, 345 (2009).
28. D. Hennings: Barium titanate based ceramic materials for dielectric use. *Int. J. High Technol. Ceram.* **3**, 91 (1986).
29. H. Chazono and M. Fujimoto: Sintering characteristics and formation mechanisms of 'core-shell' structure in $BaTiO_3$-Nb_2O_5-Co_3O_5 ternary system. *Jpn. J. Appl. Phys.* **34**, 5354 (1995).

https://doi.org/10.1557/jmr.2012.255 Published online by Cambridge University Press